Performance Analysis of Polymer Hollow Fibre Integrated Evaporative Cooling System with the Fibre Bundles in a Circular Module for Building Application

Xiangjie Chen[1,3], Yuehong Su[1], Devrim Aydin[1], Xingxing Zhang[2], Yate Ding[1], David Reay[4], Richard Law[4], Saffa Riffat[1]

[1]Department of Architecture and Built Environment, University of Nottingham, University Park, NG7 2JQ, Nottingham. United Kingdom

[2]Department of Energy, Forest and Built Environments, Dalarna University, Falun, Sweden

[3]Department of Energy and Power Engineering, University of Shanghai for Science and Technology, Jungong Road No. 516, Shanghai, 200031, China

[4]David Reay & Associates, United Kingdom

Contact: Xiangjie Chen; Email:xiangjie.chen@nottingham.ac.uk

Abstract: Due to the advantages of light weight, corrosion resistant and low cost, hollow fibres have been studied as the substitute for metallic materials. A novel hollow fibre integrated evaporative cooling system, in which the hollow fibre module constitutes as the humidifier and the evaporative cooler, is proposed. This novel hollow fibre integrated evaporative cooling system will provide a comfortable indoor environment for hot and dry area. Moreover, the water vapour can permeate through the hollow fibre effectively, and the liquid water droplets will be prevented from mixing with the processed air. In order to avoid the flow channelling or shielding of adjacent fibres, the fibres inside each bundle were made into a spindle shape to allow maximum contact between the air stream and the fibre. The cooling performances of the proposed novel polymer hollow fibre integrated evaporative cooling system were experimentally investigated under the incoming air temperature in the range of 26 ˚C to 32 ˚C and relative humidity of 25% to 35%. The effects of air velocities on the cooling effectiveness, heat and mass transfer coefficients, specific water consumption and pressure drop across the polymer hollow fibre module were analysed. Two sets of experimentally derived non-dimensional heat and mass transfer correlations were summarized, which could be favourable for the future design of polymer hollow fibre integrated evaporative cooling system.

Key words: Polymer hollow fibre, evaporative cooling, heat transfer, mass transfer, experiment

Nomenclature

A	Heat transfer area (m^2)
c_p	Specific heat (J/kg K)
d	fiber diameter (m)
h	Enthalpy (kJ/kg)
k	Thermal conductivity (W/mK)
L	Length of hollow fibre bundle (m)
m	Mass flow rate (kg/s)
N	Number of fibres inside the heat exchanger

NTU Number of heat transfer unit

Nu Nusselt number

ΔP Pressure drop (Pa)

Pr Prandtl number

q Heat transfer rate (W)

Re Reynolds number

Sc Schmidt number

T Temperature (˚C)

U Overall heat transfer coefficient (W/m^{2}K)

v Air velocity (m/s)

Greek Letters/Subscripts

a air

e evaporated water

ε Cooling effectiveness

i Inside

λ Packing fraction of a PHFHE

H Heat transfer

M Mass transfer

ρ Density of the fluid (kg/m^3)

o Outside

s Surface

μ Dynamic viscosity of the fluid(kg/ms)

ω Absolute humidity (kg/kg)

w water

wb wet bulb

v1 saturated water vapour at the entrance of the hollow fibre module

v2 saturated water vapour at the exit of the hollow fibre module

v incoming air velocity, m/s;

1. Introduction

With the rapid development of urbanization and urban sprawl, the world metropolitan areas are becoming significantly hotter due to intensive human activities. Together with the ever-increasing global warming, the energy demand for air conditioning in the world has soared dramatically during the past few decades. A recent literature review by Frontczak and Wargocki[1] indicated that thermal comfort had been regarded as the most important indoor environmental factor compared with acoustic and visual comfort. According to[2], in Europe, 6% of office, commercial and industry buildings are air-conditioned, with a total volume of 20 million cubic meters. In hot and humid climatic conditions, air conditioning system accounts for more than 50% of the total building energy consumption[3,4].

In the global market, the conventionally-used air conditioning system is based upon the mechanical vapour compression cycle. The electricity required to power the vapour compression system is most commonly generated by the combustion of primary energy (coals and fossil fuels), which is associated with the emission of global warming gases (carbon dioxide, nitrogen oxide, sulphur oxides, etc). Moreover, conventional vapour compression systems currently use HFC refrigerants, which potentially lead to the global warming and depletion of the Earth's ozone layer.

Many attempts have been made by researchers with the aim to replace mechanical vapour compression system with other environmental friendly air conditioning system with low carbon emission. With the advantages of utilization low grade energy and environmental benign refrigerants, and simple in construction, air conditioning systems such as sorption system, ejector cooling system and evaporative cooling system have been proposed and demonstrated in many niche applications[5-8]. Adsoprtion or absorption system[7] and ejector system[6] could be driven by low grade energy or industrial waste heat. However, these systems contain many components which sometimes cannot easily be manipulated. Besides, the performance of these systems are relatively low (COP around 0.2-0.5), which remains to be a major drawback for the wide application in the market. With water as the major working fluid and driven by the latent heat of evaporation, evaporative cooling system serves as another sustainable alternative for air conditioning technology. Recently, evaporative cooling system has been studied extensively by researchers, with focus on pad incorporated evaporative cooling system[9-12], desiccant based evaporative cooling system[13,14], and dew point based evaporative cooling system[15-18]. Due to the large contact surface area, porous pad incorporated evaporative cooling systems have attracted more attentions. Wu et al.[19] presented a simplified mathematical model to describe the heat and moisture transfer between water and air in a direct evaporative cooler, with pad thickness of 125mm and 260mm, the cooling efficiency reached 58% and 90% respectively. Franco et al. [20] studied the influence of water and air flows on the performance of cellulose media. The results showed that with a thickness of 85mm, a plastic grid pad could offer a cooling efficiency of 65% at wind speed of 1.5m/s. However, since water is directly in contact with the incoming air in the closed system, there is the potential for microbial growth due to the supply of stagnant water. This will provide an opportunity for the spread of liquid phase-born bacterial diseases for occupants[21].

In order to solve this problem, the hollow fibre integrated evaporative cooling system[22] has been proposed. Compared with porous pad media, hollow fibre materials provide several advantages as following: 1) allow selective permeation of moisture: with pore sizes less than 0.1μm, hollow fibre material will allow the water vapour transfer but eliminate the bacteria and fungi penetration[23]; 2) provide large surface area per unit volume[24], which is favourable for enhanced heat and mass transfer. According to Chen et al.[25], the overall heat transfer coefficients could reach up to 1675W/m^{2}K with a fibre diameter of 550μm. Kachhwaha and Preahhakar[26] analysed heat and mass transfer performance for a direct evaporative cooler using a thin plastic plate. The experimental testing results indicated that the outlet air temperatures were between 21◦C and 23◦C, at the inlet dry bulb temperature of 24.8-28.4◦C, the air humidity ratio of 2.3-5.8g/kg and air mass flow rate of 0.13, 0.2, 0.3 and 0.4g/s. Zhang[27]

proposed the theoretical investigations on a rectangular cross-flow hollow fibre membrane module for air humidification. With 2600 fibres (fibre outside diameter 1.5mm) inside the module, the outlet air temperature could reach 21.5◦C when the inlet dry bulb temperature was 30◦C. Johnson et al.[21] studied the heat and mass transfer of a hollow fibre membrane evaporative cooling system. With a different range of fibre bundles (9, 19, 29 fibre bundles), the heat transfer area was in the range of 0.35m^2-1.13m^2, and around 0.4◦C temperature drop could be observed from the experiments.

A summary of the recent experimental and modelling works on evaporative cooling system is presented in Table 1. Literature review conducted show that most of the research works have been concentrated on the theoretical analysis of polymer hollow fibre integrated evaporative cooling system. The experimental investigations for hollow fibre integrated evaporative cooling system were hardly revealed, and few testing results were available from the literature. The only detailed experimental work for polymer hollow fibre integrated evaporative cooling system was presented by Johnson et al.[21]. However the small scale testing rig only contained 29 fiber bundles, which was arranged in a curtain shape configuration. This paper presents a novel polymer hollow fibre integrated evaporative cooling system, with 3000 hollow fibers formed into a circular module. The cooling performance of the proposed system were analysed under the incoming air temperature in the range of 26℃ to 32℃ and relative humidity of 25% to 35%. The variations of saturation effectiveness and NTU were studied by varying the incoming air velocity from 0.1m/s to 4.5m/s. The effects of air velocities on the cooling effectiveness, heat and mass transfer coefficients, specific water consumption and pressure drop across the polymer hollow fibre module were analysed. Two sets of experimentally derived non-dimensional heat and mass transfer correlations were summarized and compared with the results obtained from the literature. These sets heat and mass transfer correlations could be favourable for the future design of polymer hollow fibre integrated evaporative cooling system.

Reference	Research method	Evaporative cooler type/materials	Inlet air temperature	Outlet air temperature	Wet bulb effectiveness	Conclusions
Wu et al. [19]	Simulation(simplified model)	Direct evaporative cooler/ Porous honeycomb paper	27-37◦C	23-28◦C	0.6-1.0	1) Frontal air velocity and pad thickness of the module are two key factors for the evaporative cooling system 2) The optimum frontal velocity was 2.5m/s
Anisimov et al. [28]	Simulation (ε-NTU method)	Indirect evaporative cooler/ Porous media	25-45◦C	20-30◦C	0.45-0.85	1) The novel combined parallel and regenerative counter-flow evaporative cooler could achieve lower outlet air temperature and higher cooling capacity; 2) The optimization criteria allow to establish pareto-optimal operational condition
Lin et al. [29]	Experiment+ Simulation (ε-NTU method)	Dew point evaporative cooler/ hydrophobic material	22-30◦C	25-18◦C	0.6-1.0	1) The saturation point of the working air is influenced by the working air ratio and channel height; 2) Overall heat transfer coefficient could achieve higher than 100W/m^2K

Jradi and Riffat [30]	Experiment+ Simulation (finite difference scheme)	Dew point evaporative cooler/ Porous membrane media	23-40◦C	18-30◦C	0.6-1.12	The optimized design of the dew point cooler could provide 1.12 wet bulb effectiveness and 0.78 dew point effectiveness
Zhang [31]	Experiment+ Simulation (fractal theory)	Direct evaporative cooler/hollow fiber membrane	NA	NA	NA	1) Experimental obtained relationship between Sherwood and Reynolds number was established using fractal model; 2) Membrane module with higher packing fraction could lead to better heat transfer performance.
Franco et al. [20]	Simulation	Direct evaporative cooler/ Porous paper	NA	NA	0.6-0.8	1)Comparisons of the cooing performance of five different porous materials revealed that the plastic grid block produced highest efficiency of 82.6% 2) Higher efficiency will lead to lower specific water consumption
Zhao et al. [32]	Simulation	Dew point evaporative cooler/ Porous polygonal stack	28◦C	NA	0.5-1.3	1)Cooling effectiveness increases with increasing working-to-intake air ratio 2)Under UK summer design condition, the wet-bulb and dew-point effectiveness could reach up to 1.3 and 0.9
Anisimov et al. [33]	Experiment+ Simulation	M-cycle cross flow indirect evaporative cooler	20-44◦C	18.4-23.8◦C	0.8-1.2	1) M-cycle cross flow indirect evaporative cooler is more suitable for use in hot and dry climate 2) Cooling capacity varied between 1 and 19kW for every kg/s of air flow.

2. Theory

Considering the polymer hollow fibre material as a porous medium through which flows of air and water pass, the following expressions[21] were used to characterize their functioning based on heat and mass balance between the air flow and the porous fibre medium. The schematic diagram of the system is shown in Figure 1.

The basic heat and mass transfer equation:

$$q = m_a C_{pa}(T_1 - T_2) + m_a[\omega_1(h_{v1} - h_{wb}) - \omega_2(h_{v2} - h_{wb})] \quad \text{Eq.(1)}$$

$$m_e = m_a(\omega_2 - \omega_1) \quad \text{Eq.(2)}$$

Where q is the flow of transferred heat (W);

m_e is the flow of evaporated water(kg/h);

c_{pa} is the specific heat of dry air (kJ/kg K);

T_1 is the dry bulb temperature of the incoming air (◦C);

T_2 is the dry bulb temperature of the outgoing air (◦C);

h_{v1} and h_{v2} are the enthalpy of saturated water vapour at the entrance and exit of the hollow fibre module (kJ/kg);

h_{wb} is the enthalpy of saturated water vapour at the wet bulb temperature of the incoming air (kJ/kg);

m_a is the mass flow rate of the incoming air (kg/h);

ω_1 is the relative humidity of the incoming air;

ω_2 is the relative humidity of the outgoing air.

The flow of transferred heat (q) and the flow of evaporated water (m_e) could be expressed as the product of heat transfer coefficient and the mean logarithmic difference in temperature (ΔT), and the product of the mass transfer coefficient and the mean logarithmic difference in the water vapour density ($\Delta\rho_V$). These can be expressed in the following two equations:

$$q = h_H A_s \Delta T \quad \text{Eq.(3)}$$

$$m_e = h_M A_s \Delta\rho_V \quad \text{Eq.(4)}$$

Where h_H is the coefficient of heat transfer (W/m^{2}K);

h_M is the coefficient of mass transfer (W/m^{2}K);

A_s is the total surface area of the hollow fibre (m^2);

The mean logarithmic difference in temperature (ΔT) and water vapour density ($\Delta\rho_V$) can be calculated using following equations:

$$\Delta T = \frac{(T_2 - T_1)}{\ln(\frac{T_2 - T_{wb}}{T_1 - T_{wb}})} \quad \text{Eq.(5)}$$

$$\Delta\rho_V = \frac{(\rho_{V2} - \rho_{V1})}{\ln(\frac{\rho_{V1} - \rho_{wb}}{\rho_{V2} - \rho_{wb}})} \quad \text{Eq.(6)}$$

Where $\rho_{V1}$and ρ_{V2} are the water vapour density on entering and leaving the hollow fibres (kg/m^3);

ρ_{wb} is the saturated water vapour density at the wet bulb temperature (kg/m^3).

The heat and mass transfer coefficients could be expressed as:

$$h_H = \frac{Nu * k}{L} \quad \text{Eq.(7)}$$

$$h_M = \frac{Sh * D_{AB}}{L}$$ Eq.(8)

Where k is the thermal conductivity of the water (W/mK);

L is the characteristic length of the hollow fibre bundle.

The relationship between Reynolds number (Re), Prandtl number (Pr) and Nusselt number (Nu), and the relationship between Reynolds number (Re), Schmidt number (Sc)and Sherwood number (Sh) can be expressed by:

$$Nu = C1Re^{m1}Pr^{1/3}$$ Eq.(9)

$$Sh = C2Re^{m2}Sc^{1/3}$$ Eq.(10)

Where C1,C2, m1, m2 are constants for the hollow fibre bundles.

Reynolds number can be calculated by:

$$\mathrm{Re} = \frac{v * d_h}{\mu}$$ Eq.(11)

Where v is the incoming air velocity, m/s;

d_h is the hydraulic diameter of the hollow fibre module, m;

μ is the viscosity of the incoming air, m^2/s.

The wet-bulb effectiveness (ε_{wb}) and the dew point effectiveness (ε_{dew}) are important expressions used to characterise the air saturation capacity of the polymer hollow fibre bundle. The wet-bulb effectiveness (ε_{wb}) is used to indicate how close the outlet temperature of product air to the inlet wet-bulb temperature of the working air. ε_{wb} can be defined as the ratio between the temperature difference on passing through the hollow fibre bundle ($T_1 - T_2$) and the maximum temperature difference that would occur if the air were saturated ($T_1 - T_{wb}$):

$$\varepsilon_{wb} = \frac{T_1 - T_2}{T_1 - T_{wb}}$$ Eq.(12)

The dew point effectiveness (ε_{dew}) compares the difference of the inlet and outlet air dry bulb temperature ($T_1 - T_2$) between its inlet dry-bulb temperature and the inlet dew point temperature ($T_1 - T_{dew}$):

$$\varepsilon_{dew} = \frac{T_1 - T_2}{T_1 - T_{dew}}$$ Eq.(12)

The sensible cooling capacity of the hollow fiber integrated evaporative cooling system can be expressed by:

$$Q_s = m_a C_{pa} \Delta T = m_a C_{pa}(T_1 - T_2)$$ Eq.(13)

Where m_a is the mass flow rate of the incoming air (kg/h);

c_{pa} is the specific heat of dry air (kJ/kg K);

$\Delta T = T_1 - T_2$, is the temperature drop of the incoming air (◦C).

The latent cooling capacity of the hollow fiber integerated evaporative cooling system can be calculated by:

$$Q_l = m_a h_{fg} \Delta\omega = m_a h_{fg}(\omega_1 - \omega_2) \quad \text{Eq.(14)}$$

Where h_{fg} is the specific latent heat of water evaporation (kJ/kg);

$\Delta\omega = \omega_1 - \omega_2$ is the moisture addition ratio of the incoming air (g/kg).

Where m_{air} is the incoming air mass flow rate, h_1 and h_2 are the enthalpy of the inlet and outlet air.

The amount of water evaporated from the hollow fibre bundle can be expressed as the mass flow of evaporated water per unit of exposed surface (A_f) and the thermal difference that can be achieved for given air conditions on entering the materials:

$$C_w = \frac{m_e}{(T_1 - T_2)A_f} \quad \text{Eq.(15)}$$

Where A_f is the total surface area of the hollow fibre bundles.

3. Apparatus and procedure

An experimental testing rig was developed to determine the heat and mass transfer coefficients and cooling effectiveness of the polymer hollow fibre integrated evaporative cooling system. Polyvinylidene fluoride (PVDF) hollow fibres (manufactured by ZENA Ltd.) with outside diameter of 0.8mm and inside diameter of 0.6mm, an effective pore size of 0.5μm and a porosity of 50% were used for the fabrication of the polymer hollow fibre module. The testing rig comprises a circular shape polymer hollow fibre module, an air tunnel, a water pump, a fan, a water filter and a water tank. The detailed schematic diagram is shown in Figure 1. A 8-litre water tank was used to provide water circulation inside the fibre. In order to avoid any particle blockage within the polymer hollow fibres, a water filter was allocated before the entrance of the hollow fiber module to improve the purity of the incoming water into the fibres. A flow meter and a ball valve were included in the water circulation cycle with the aim to control the water flow rate inside the fibre. In order to minimize the experimental testing errors, four humidity and temperature sensors (EK-H4, Sensirion, UK) were located at the inlet (point 1 in Figure 1) and outlet (point 2 in Figure 1) of the air stream respectively, to measure the inlet and outlet conditions of the air stream. The actual locations of the sensors are shown in Figure 3. Additional K type thermocouples were used to measure the water temperature entering and leaving the hollow fibre module (point 3 and 4 in Figure 1). The aluminium air tunnel was connected with a variable frequency drive centrifugal fan, which was linked directly with the environmental chamber. A centrifugal pump was employed to circulate water from the water tank to the top of the hollow fiber module. 8 nozzles were allocated at the top of the module with the aim to make sure the cross section of the hollow fiber module could be wetted entirely.

The circular shape polymer hollow fibre module consists of 3000 fibres, which were sealed at each ends to a plastic plate using superglue sealant. The height of the polymer hollow fibre module was 0.6m, while the cross section diameter of the module was 0.4m. Buffer?? The hollow fibre module was incorporated into a circular aluminium tunnel, whose cross section diameter was 0.15m. The detailed

3-D model and the actual testing prototype image of the hollow fibre module is shown in Figure 2 and Figure 3 respectively. The detailed geometrical, physical properties of the polymer hollow fibre module and the experimental working conditions were summarized in Table 1.

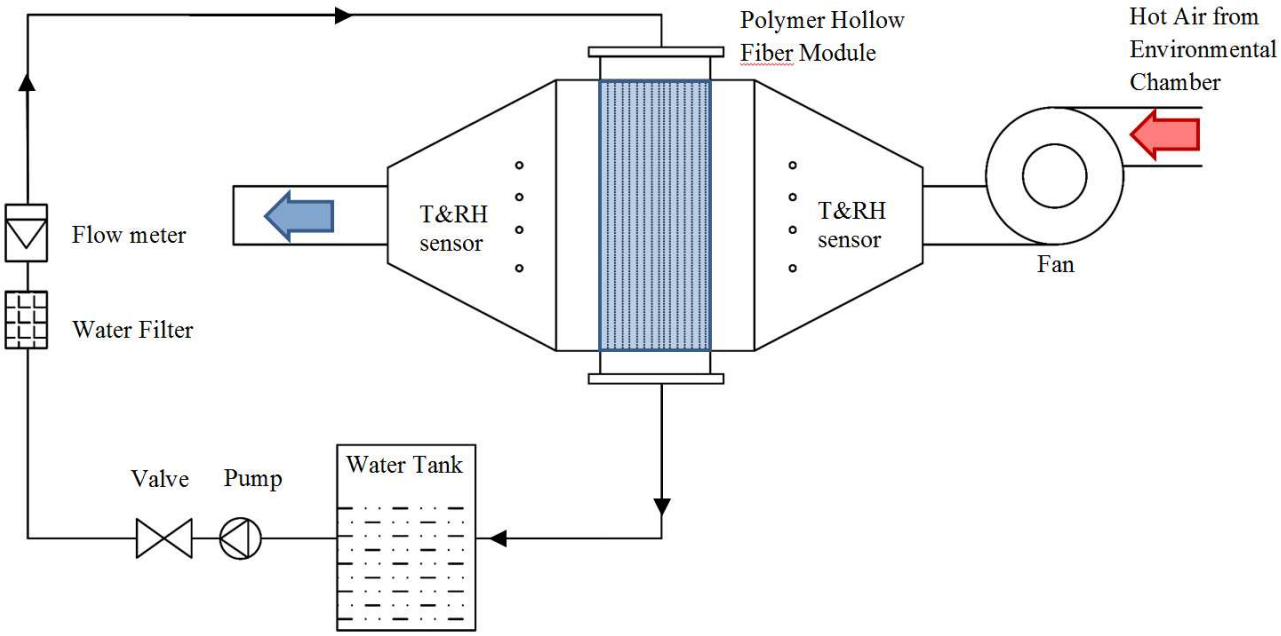

Figure 1 Schematic diagram of polymer hollow fibre integrated evaporative cooling system

Figure 2 The 3-D model image of the hollow fibre module

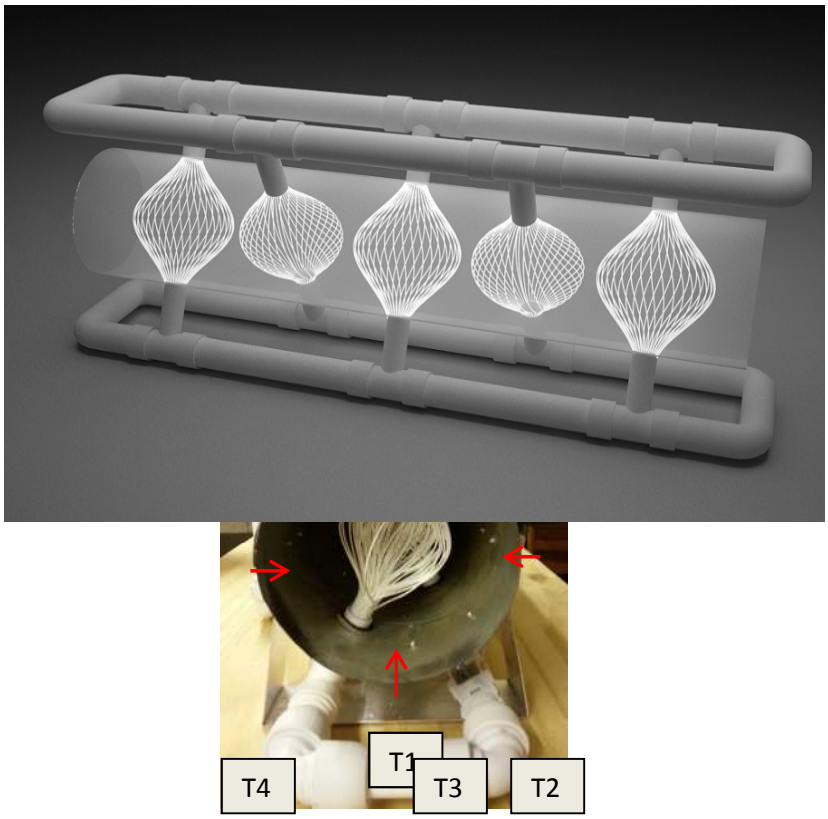

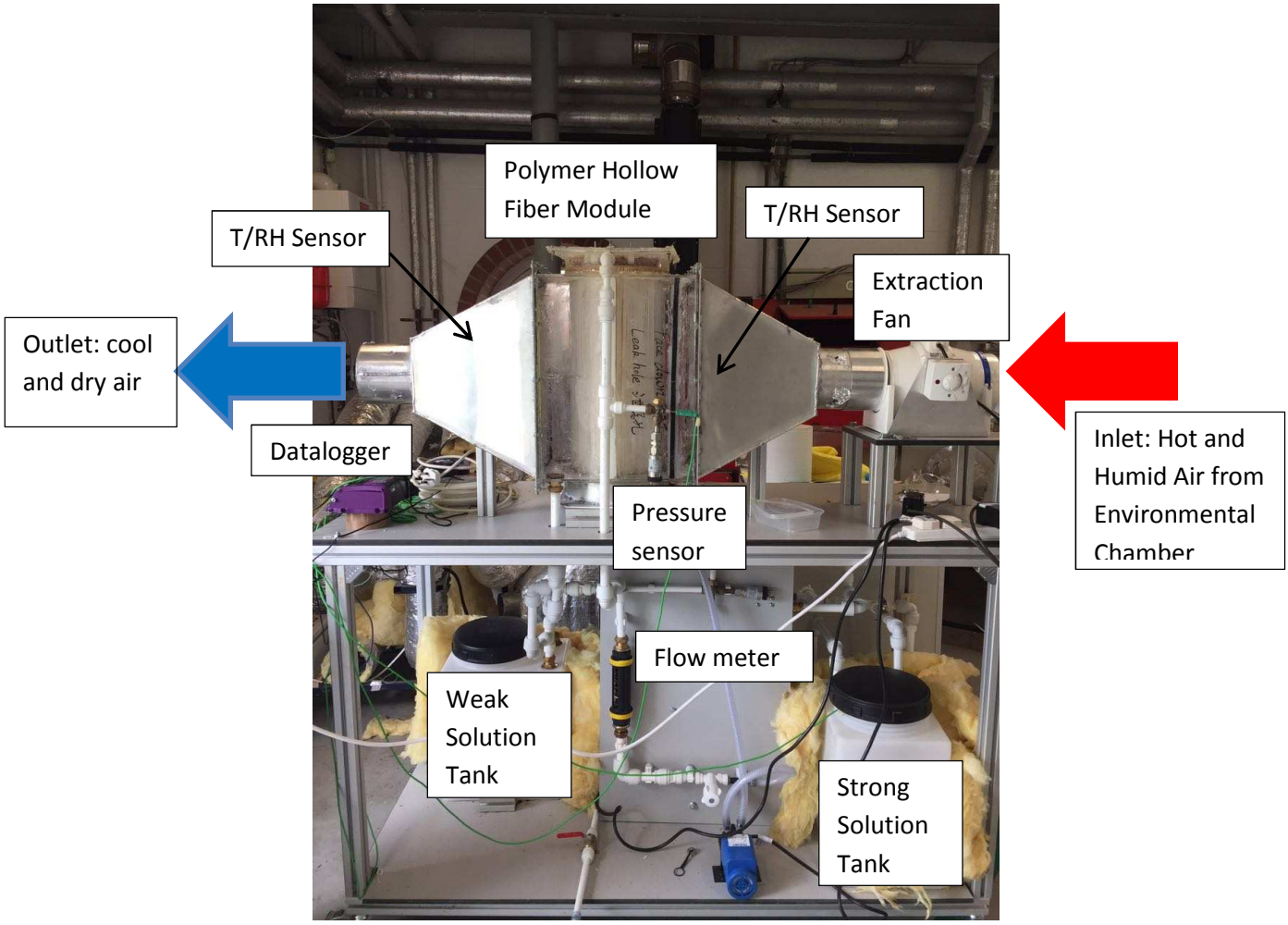
Polymer Hollow Fiber Module
T/RH Sensor
T/RH Sensor
Extraction Fan
Outlet: cool and dry air
Datalogger
Inlet: Hot and Humid Air from Environmental Chamber
Pressure sensor
Flow meter
Weak Solution Tank
Strong Solution Tank

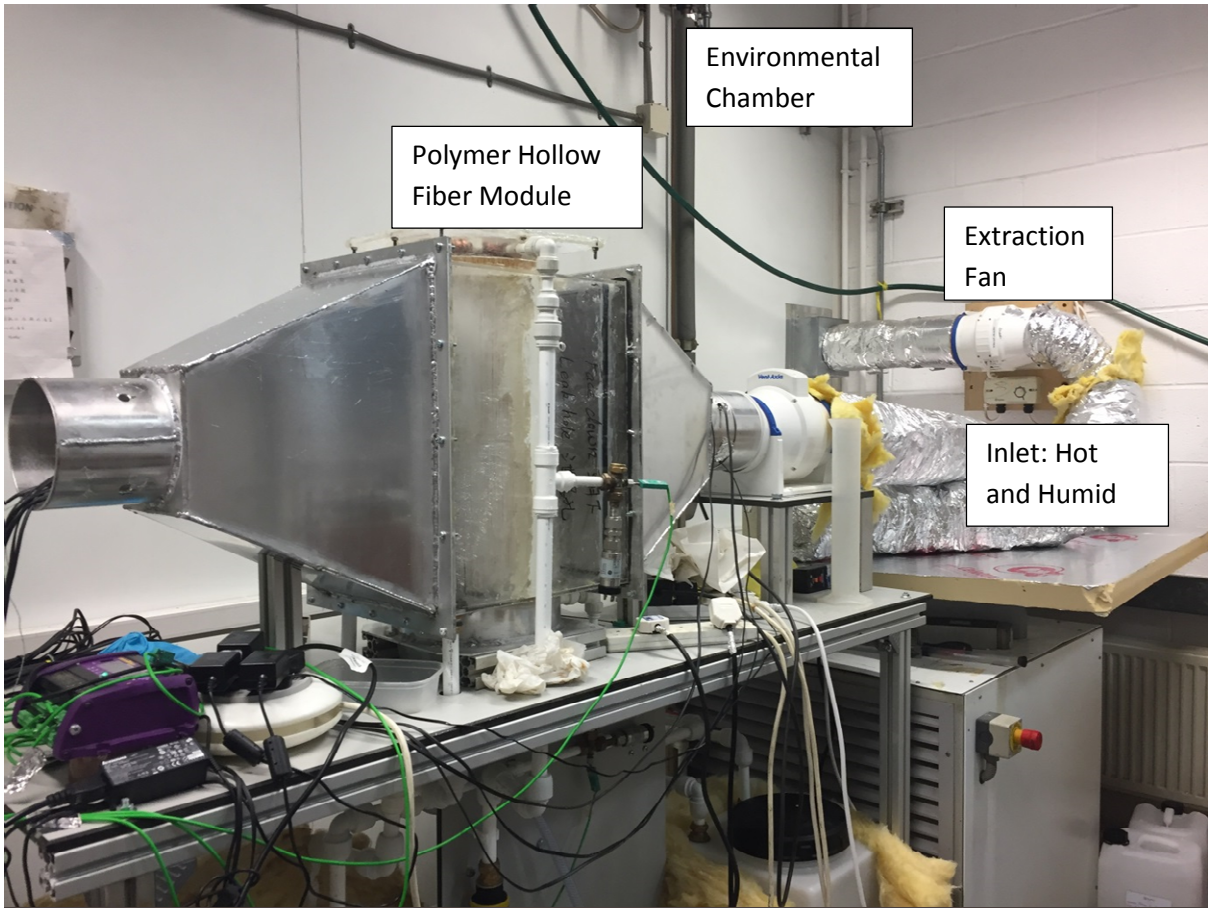

Figure 3 The cross section image of the hollow fibre module (with detailed thermocouple locations shown as T1-T4)

At the beginning of each test, the environmental chamber was set to the required temperature and humidity level. As soon as the temperature and humidity reached the desired values, the water circulation pump and the fan in the air stream direction will be switched on. The air velocity is measured at five different positions along the cross sections of the outlet aluminium tunnel, using the air velocity probes connected to a recorder (Testo 454). The dynamic pressures in the upstream and downstream of the air flow were recorded using Pressure transducers (Ge UNIK 5000).

For each test, the temperature and humidity values were recorded every 20 seconds until the time when the system reach steady states as indicated by the humidity and temperature sensor readings. The accuracy of the measuring instruments used was: ±0.2% for temperature, ±0.5% for pressure, ±2% for air velocity, and ±2% for relative humidity.

Table 1 Physical properties of the polymer hollow fibre module

Property	**Symbol**	**Values**	**Unit**
Module cross section diameter	D	0.20	m
Module height	h	0.5	m
Fibre number inside the module	N	5000	
Fibre outside diameter	d_o	0.8	mm
Fibre inside diameter	d_i	0.6	mm
Nominal pore size		0.2	µm
Fibre porosity		0.6	

Packing density		832	m^2/m^3
Packing fraction		0.32	
Polymer hollow fibre thermal conductivity	k	0.17	W/mK
Incoming air velocity	v_a	0.15-3.5	m/s
Water flow rate inside fibre	m_w	0.05	l/m
Incoming air temperature	T_a	34-35	◦C
Incoming air humidity	ω_a	23, 32, 42%	

4. Results and discussions

Experimental tests were conducted in order to analyse the cooling performance of the polymer hollow fiber integrated evaporative cooling system. The inlet air dry bulb temperature was kept in the range of 34-35◦C, with the relative humidity in the range of 23-40%. In order to make sure all the hollow fibers inside the module get wetted during the experiment, the water flow rate inside the fiber was kept at relatively high level (2l/m).

Three different testing conditions (as shown in Table 2) are identified for the experimental tests of polymer hollow fibre integrated evaporative cooling system. In order to compare the effects of different air relative humidity on the system performance, three different inlet air relative humidity (23%, 32%, 40% respectively) were determined with approximately the same inlet dry bulb temperature around 35◦C (1.2% deviation). Results analyses have been conducted on the impacts of incoming air velocity on the outlet air dry bulb temperature and relative humidity, system cooling effectiveness and cooling capacity, pressure drop, heat and mass transfer coefficients, etc.

Table 2 Typical testing data for three experimental conditions

4.1 The effect of inlet air temperature and relative humidity

4.2 The effect of inlet air velocity

Dehumidification experiments were carried out for KCOOH concertation ratio of 62%, 49% and 36%, incoming air dry bulb temperature in the range of 35-45◦C and the relative humidity of 60-70%. By varying the incoming air velocity, the moisture removal rate, the cooling capacity and the dehumidifier effectiveness were analysed and presented in this section.

The variations of moisture removal rate with respect to various incoming air velocity under solution concentration ratio of 62% and inlet air dry bulb temperature of 35◦C are illustrated in Figure 7. It can be found that the moisture removal rate increases as the inlet air velocity improves from 0.7m/s to 3.5m/s. When keep the inlet air velocity at the fixed value, higher incoming air relative humidity will lead to greater moisture removal rate. For instance, at the air velocity of 1.5m/s, the moisture removal rate is 0.235g/s, 0.36g/s and 0.56g/s respectively for incoming air relative humidity of 60%, 65% and 70%. The reason is because that higher air relative humidity represents higher vapour pressure, which means a greater vapour pressure difference between the incoming air and the desiccant solution. This will lead to greater driving force for the solution to attract moisture from the humid air. Comparison between presented data and the experimental testing result from Elmer et al.[34] was also demonstrated in Figure 7. Also using KCOOH, under incoming air temperature of 35◦C, RH=70% and solution concentration ratio of 67%, the moisture removal rate obtained by Elmer et al.[34] was 0.45g/s under the air volumetric flow rate of 243m^3/h. This result falls in well with the linear relationship for

RH=70%, T_{in}= 35◦C, ω=62%. Given the condition that Elmer et al.[34]'s solution concentration ratio is 67%, which is 4% higher than applied in this testing condition, the moisture removal effects of proposed system is obviously better than what is presented by Elmer et al.[34]

The variations of cooling capacity with respect to various incoming air velocity under solution concentration ratio of 62% and inlet air dry bulb temperature of 35◦C are shown in Figure 8. It is noted that the cooling capacity will improve as the air velocity increases. Higher incoming air relative humidity will also lead to better cooling capacity. For instance, for incoming air relative humidity of 70%, the cooling capacity is in the range of 0.86kW to 1.92kW, which is averagely 25% higher than that with RH=65%. Comparably cooling capacity of 0.68kW were obtained by Elmer et al.[34] under incoming air temperature of 35◦C, RH=70% and solution concentration ratio of 67%. Such cooling capacity (0.68kW) is corresponding to the linear relationship of RH=65% of presented data, which shows that the cooling capacity of proposed hollow fiber integrated desiccant cooling system actually out- performs Elmer et al.[34]'s

Figure 9 demonstrated variations of dehumidifier effectiveness with respect to various inlet air velocities under different incoming air relative humidity for solution concentration ratio of 62% and inlet air dry bulb temperature of 35◦C. It can be found that the dehumidifier effectiveness declines as the air velocity increases for a fixed solution concentration ratio and inlet air conditions. The reason is due to the fact that at higher incoming air velocity, the solution inside the polymer hollow has less time to get in contact with the incoming air, this consequentially leads to reduced Δω. According to Eq. (),Δω is proportionally related to the dehumidifier effectives. Hence, higher air velocity is associated with lower dehumidifier effectiveness. The experimental results presented by Elmer et al.[34] indicated that, at incoming air temperature 35◦C and RH=70%, but with higher solution concentration ratio (67%), the dehumidifier effectiveness was around 0.34, which is actually lower than the proposed hollow fiber integrated evaporative cooling system.

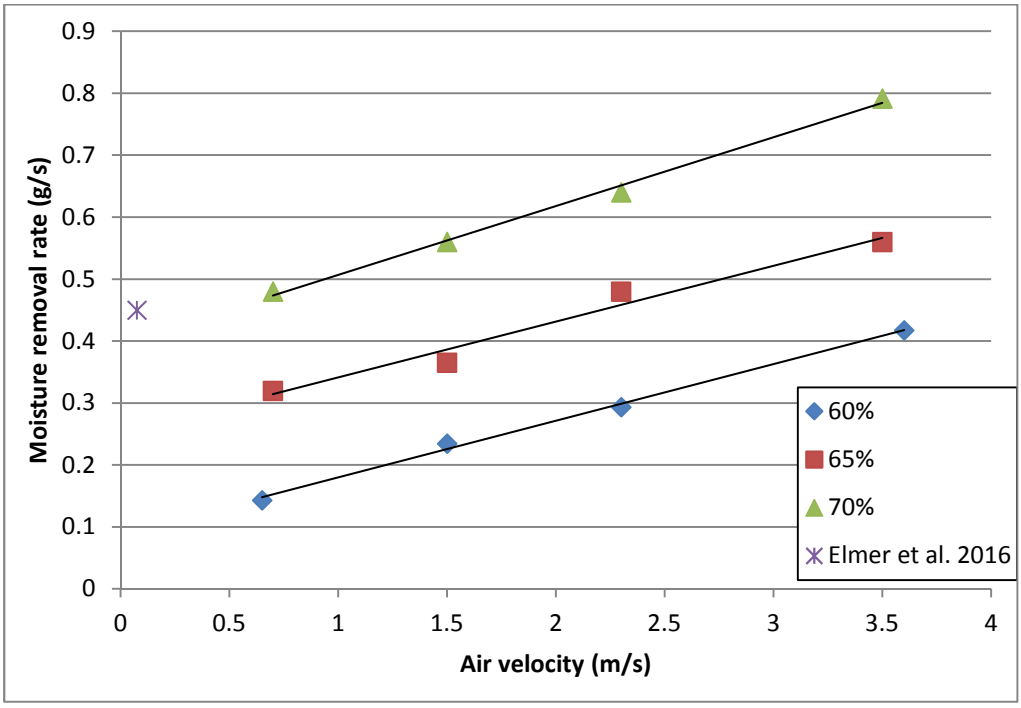

Figure 7 Variations of dehumidifier moisture removal rate with respect to various inlet air velocities under different incoming air relative humidity (T_{in}= 35◦C, ω=62%)

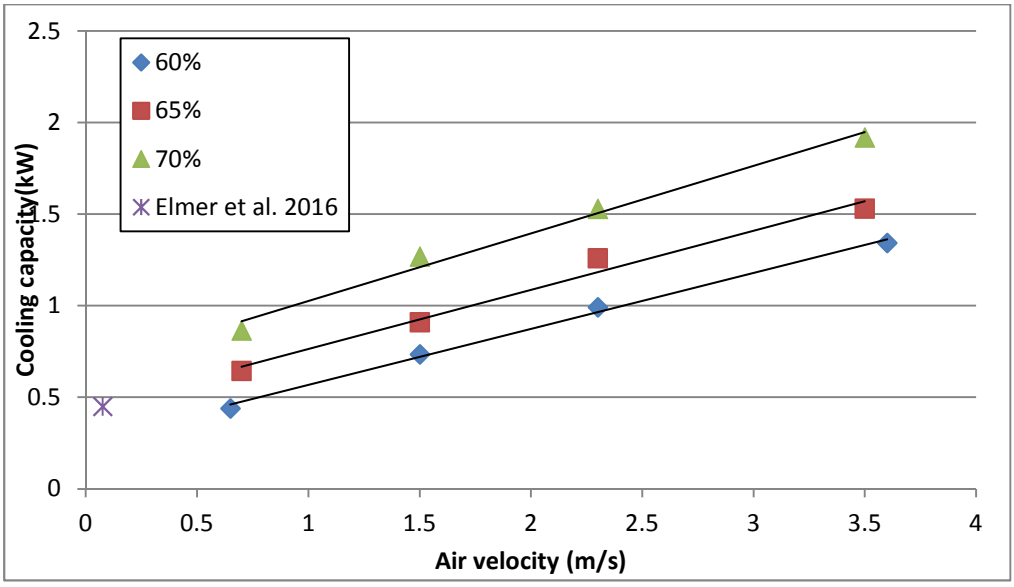

Figure 8 Variations of cooling capacity with respect to various inlet air velocities under different incoming air relative humidity (T_{in}= 35◦C, ω=62%)

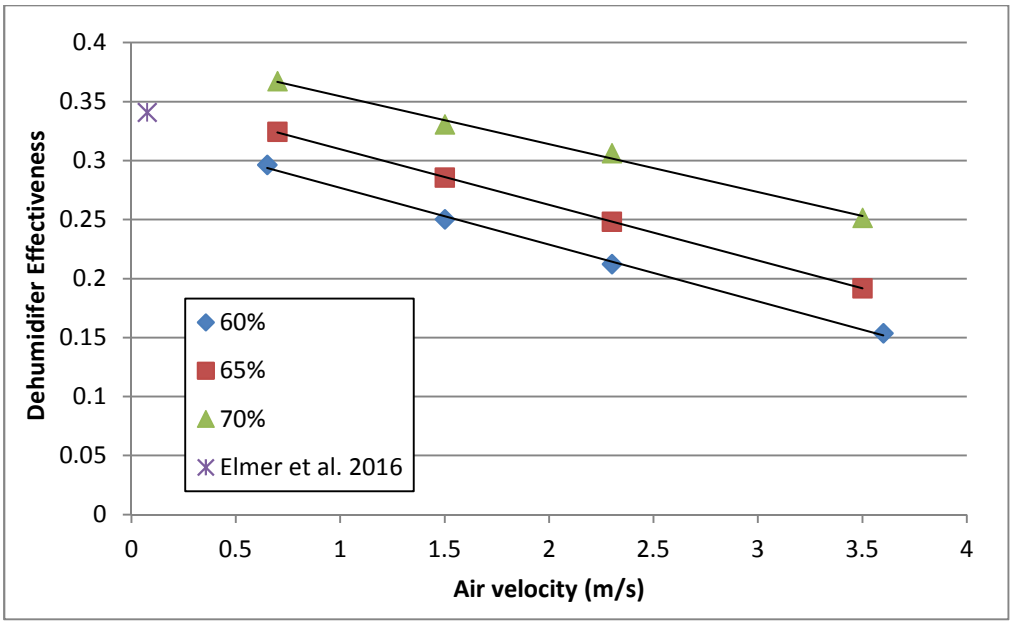

Figure 9 Variations of dehumidifier effectiveness with respect to various inlet air velocities under different incoming air relative humidity (T_{in}= 35◦C, ω=62%)

Another group of tests were conducted with the aim to investigate the effect of different solution concentration ratio on the moisture removal rate

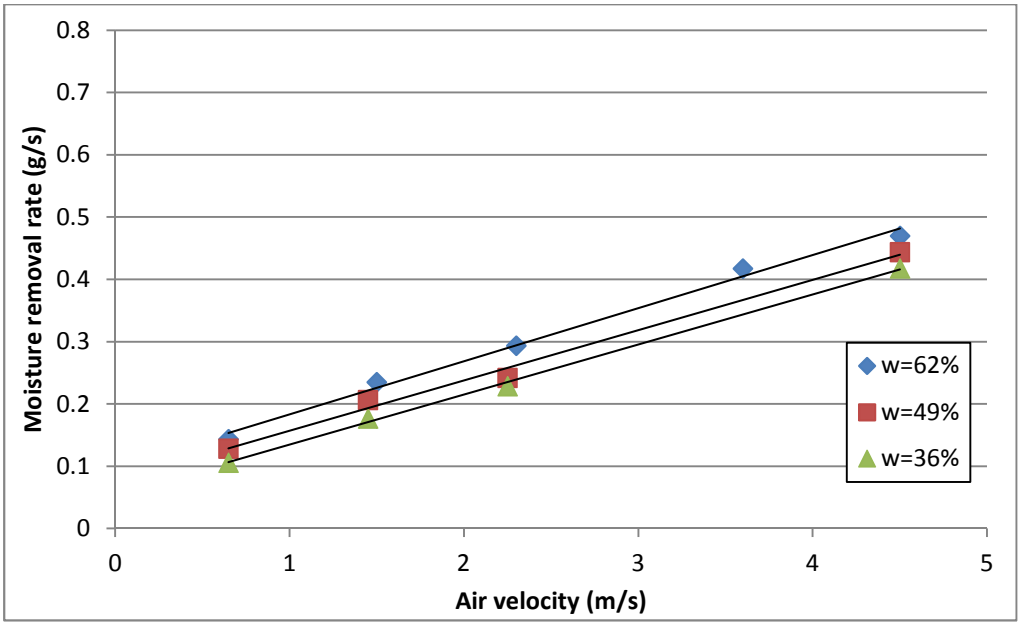

Figure 10 Variations of dehumidifier moisture removal rate with respect to various inlet air velocities under different solution concentration ratio (inlet RH=60%)

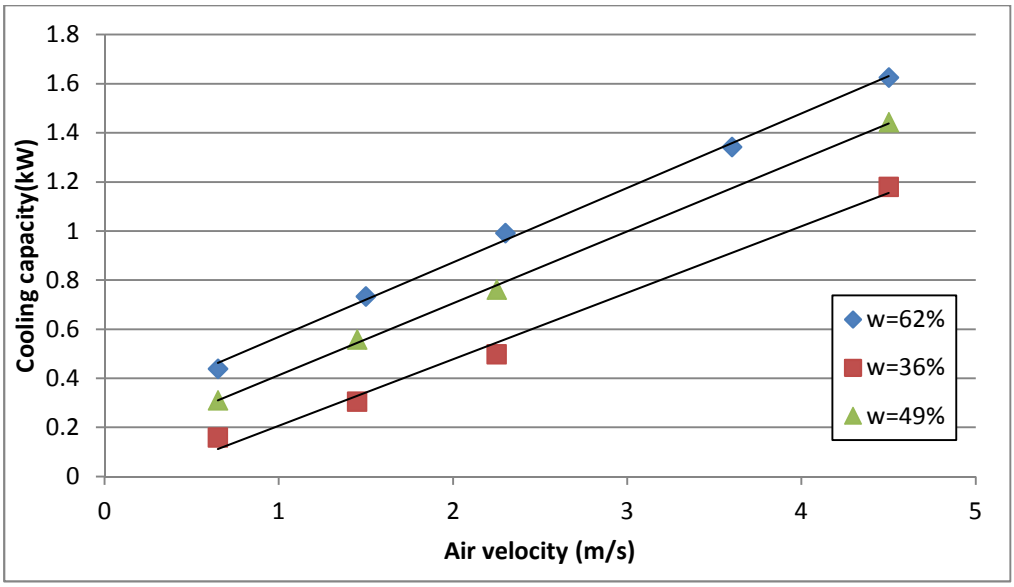

Figure 11 Variations of cooling capacity with respect to various inlet air velocities under different solution concentration ratio (inlet RH=60%)

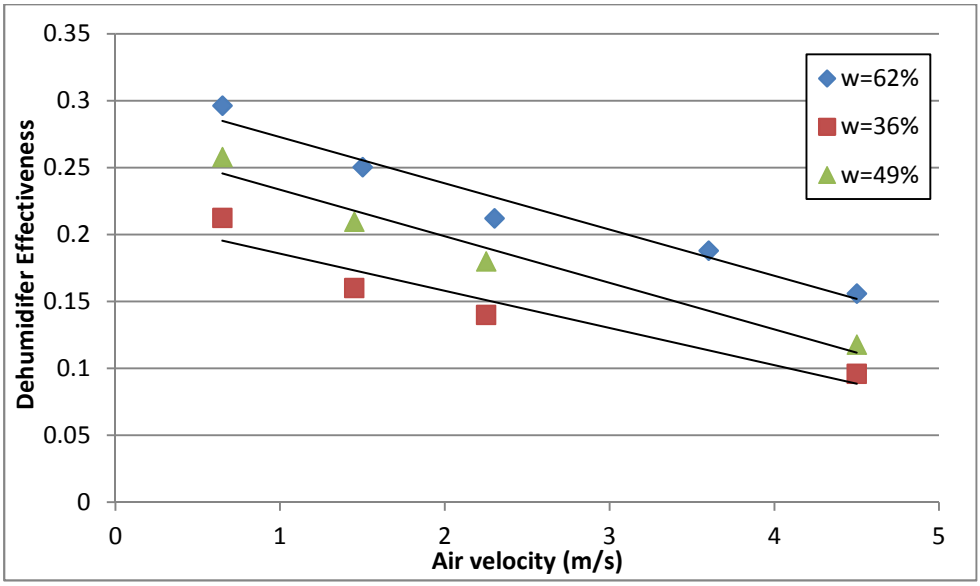

Figure 12 Variations of dehumidifier effectiveness with respect to various inlet air velocities under different solution concentration ratio (inlet RH=60%)

Figure 4 and Figure 5 illustrate respectively the distribution of the inlet and outlet air dry bulb temperature and relative humidity of one typical testing condition for the hollow fibre integrated evaporative cooling system. The system was tested under the incoming air temperature around 34.80◦C, and relative humidity of 22.65% under the air velocity of 1.5m/s. At the beginning of the tests, it took around 9 minutes for the outlet air temperature and relative humidity reached stable state condition.

4.3 The effect of inlet air relative humidity

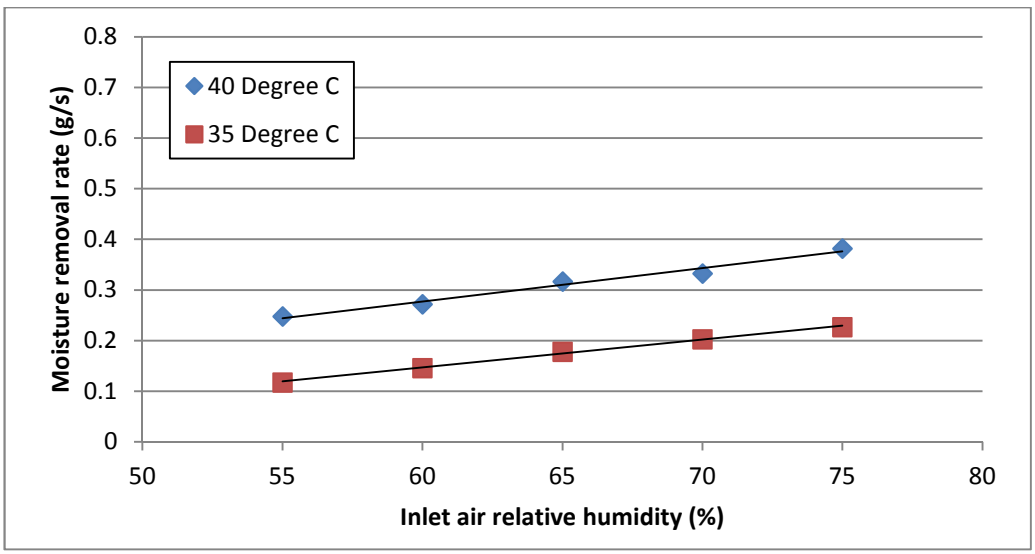

Figure 13 Variations of moisture removal rate with respect to various inlet air relative humidity under different incoming air temperature (Va=0.7m/s)

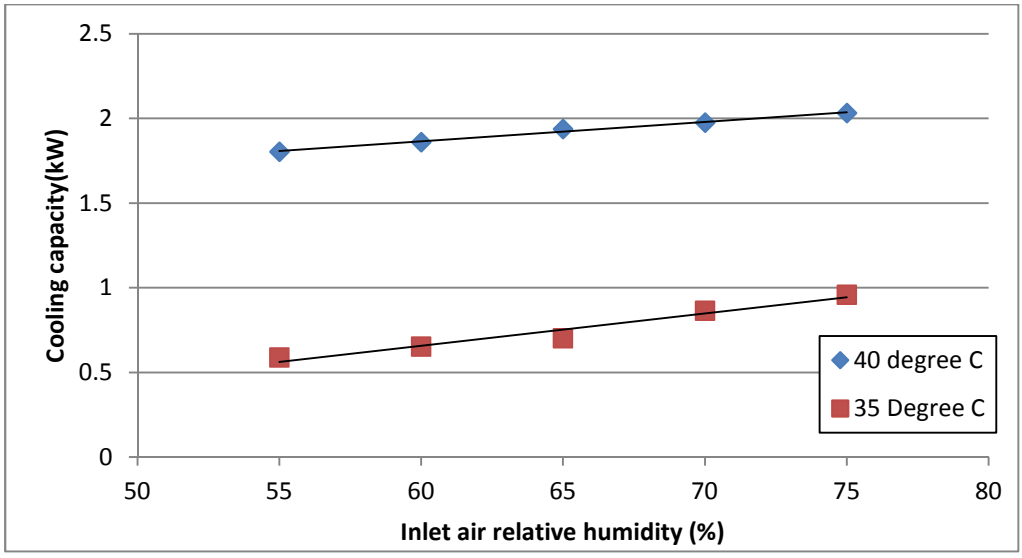

Figure 14 Variations of cooling capacity with respect to various inlet air relative humidity under different incoming air temperature (Va=0.7m/s)

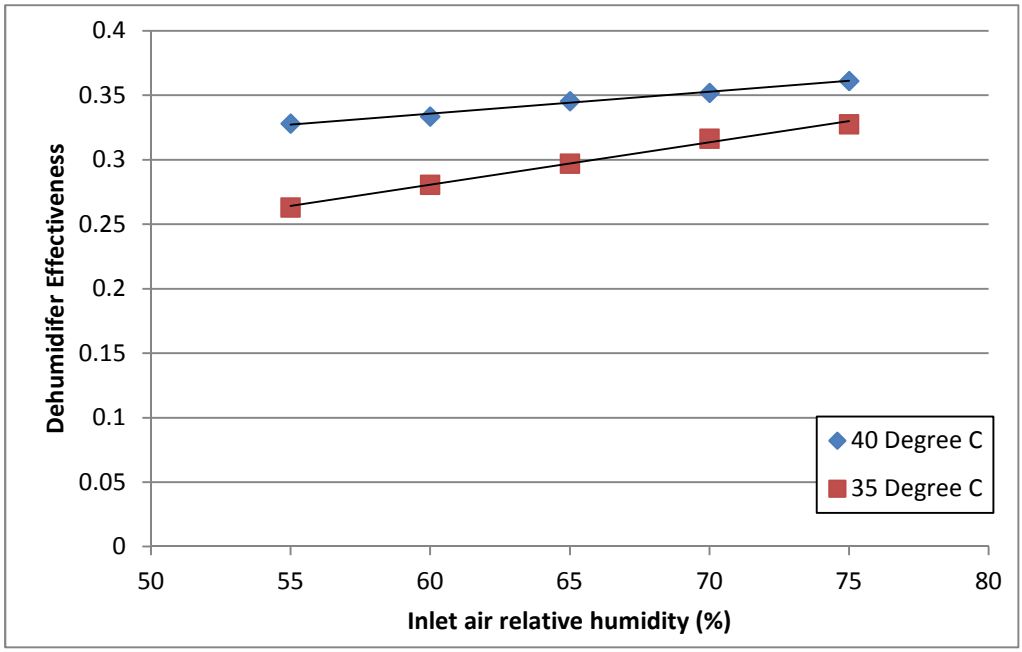

Figure 15 Variations of dehumidifier effectiveness with respect to various inlet air relative humidity under different incoming air temperature (Va=0.7m/s)

5.Conclusion

A novel hollow fibre integrated evaporative cooling system, in which the hollow fibre module constitutes as the humidifier and evaporative cooler, is proposed in this paper. In order to avoid the flow channelling or shielding of adjacent fibres, the fibres inside each bundle were made into a loose state to allow maximum contact between the air stream and the fibre. The experimental obtained cooling effectiveness, pressure drop and specific water consumption with respect to various incoming air

velocity were reported. The variations of heat and mass transfer coefficients with respect to Reynolds number under three different testing conditions are discussed. The main conclusions in this research are:

1. With inlet air temperature of 28◦C and RH of 27%, by changing the air velocity from 0.15m/s to 3.5m/s, the experimental determined air outlet temperature and RH were approximately 22.3◦C and 41% respectively. These experimental obtained values were in good agreement with the simulation results, with percentage deviations of 3.95% and 4.82% respectively.
2. By changing the air velocity from 0.15m/s to 3.5m/s, the experimental obtained cooling effectiveness deceased from 0.45 to 0.15. With air inlet dry bulb temperature more or less the same, while relative humidity difference of 7.8%, condition 1 with lower relative humidity yielded higher cooling effectiveness.
3. The experimental obtained pressure drop with respect to various air velocities was reported. The pressure drop increased from 0.45Pa to 2.1Pa as the air velocity improved from 0.15m/s to 3.5m/s. These values were about 10-40% of the pressure drops obtained by Zhang[27], in which the fibre numbers were 4 to 10 times higher than our proposed system.
4. With the Reynolds number in the range of 10-160, the heat and mass transfer coefficients were in the range of 25-170W/m^{2}K and 0.04-0.25m/s. Two sets of non-dimensional heat and mass transfer correlations with respect to Reynolds number were deviated from the experimental results, which showed good agreements with other correlations from literature.

The experimental results of polymer hollow fibre integrated evaporative cooling system demonstrated very comparable cooling performance with respect to other porous media integrated evaporative cooling. Future research could be concentrated on changing the fibre module configurations (including changing the fibre pores size with thinner fibre walls, increasing the fibre number or using chaos type fibre, etc) to increase the heat and mass transfer performance.

Acknowledgement

The authors would like to acknowledge the financial support and contributions from Innovate UK (project code: 131821).

Reference

1 Frontczak, M. & Wargocki, P. Literature survey on how different factors influence human comfort in indoor environments. *Building and Environment* **46**, 922-937, doi:https://doi.org/10.1016/j.buildenv.2010.10.021 (2011).

2 Directive 2010/31/EU of 19 May 2010 on the energy performance of buildings. *European Commission 2010/31/EU (EPBD)* (2010).

3 Pérez-Lombard, L., Ortiz, J. & Pout, C. A review on buildings energy consumption information. *Energy and Buildings* **40**, 394-398, doi:http://dx.doi.org/10.1016/j.enbuild.2007.03.007 (2008).

4 Lior, N. Sustainable energy development (May 2011) with some game-changers. *Energy* **40**, 3-18, doi:https://doi.org/10.1016/j.energy.2011.09.044 (2012).

5 Chen, X., Worall, M., Omer, S., Su, Y. & Riffat, S. Theoretical studies of a hybrid ejector CO2 compression cooling system for vehicles and preliminary experimental investigations of an ejector cycle. *Applied Energy* **102**, 931-942, doi:http://dx.doi.org/10.1016/j.apenergy.2012.09.032 (2013).

6 Chen, X., Omer, S., Worall, M. & Riffat, S. Recent developments in ejector refrigeration technologies. *Renewable and Sustainable Energy Reviews* **19**, 629-651, doi:10.1016/j.rser.2012.11.028 (2013).
7 Wang, R. Z. & Oliveira, R. G. Adsorption refrigeration—An efficient way to make good use of waste heat and solar energy. *Progress in Energy and Combustion Science* **32**, 424-458, doi:https://doi.org/10.1016/j.pecs.2006.01.002 (2006).
8 Duan, Z. *et al.* Indirect evaporative cooling: Past, present and future potentials. *Renewable and Sustainable Energy Reviews* **16**, 6823-6850, doi:https://doi.org/10.1016/j.rser.2012.07.007 (2012).
9 Farmahini-Farahani, M., Delfani, S. & Esmaeelian, J. Exergy analysis of evaporative cooling to select the optimum system in diverse climates. *Energy* **40**, 250-257, doi:http://dx.doi.org/10.1016/j.energy.2012.01.075 (2012).
10 Liao, C.-M. & Chiu, K.-H. Wind tunnel modeling the system performance of alternative evaporative cooling pads in Taiwan region. *Building and Environment* **37**, 177-187, doi:http://dx.doi.org/10.1016/S0360-1323(00)00098-6 (2002).
11 Rawangkul, R., Khedari, J., Hirunlabh, J. & Zeghmati, B. Performance analysis of a new sustainable evaporative cooling pad made from coconut coir. *International Journal of Sustainable Engineering* **1**, 117-131, doi:10.1080/19397030802326726 (2008).
12 He, S. *et al.* Experimental study of film media used for evaporative pre-cooling of air. *Energy Conversion and Management* **87**, 874-884, doi:http://dx.doi.org/10.1016/j.enconman.2014.07.084 (2014).
13 Mujahid Rafique, M., Gandhidasan, P., Rehman, S. & Al-Hadhrami, L. M. A review on desiccant based evaporative cooling systems. *Renewable and Sustainable Energy Reviews* **45**, 145-159, doi:http://dx.doi.org/10.1016/j.rser.2015.01.051 (2015).
14 Alahmer, A. Thermal analysis of a direct evaporative cooling system enhancement with desiccant dehumidification for vehicular air conditioning. *Applied Thermal Engineering* **98**, 1273-1285, doi:http://dx.doi.org/10.1016/j.applthermaleng.2015.12.059 (2016).
15 Riangvilaikul, B. & Kumar, S. An experimental study of a novel dew point evaporative cooling system. *Energy and Buildings* **42**, 637-644, doi:http://dx.doi.org/10.1016/j.enbuild.2009.10.034 (2010).
16 Caliskan, H., Hepbasli, A., Dincer, I. & Maisotsenko, V. Thermodynamic performance assessment of a novel air cooling cycle: Maisotsenko cycle. *International Journal of Refrigeration* **34**, 980-990 (2011).
17 Zhao, X., Li, J. M. & Riffat, S. B. Numerical study of a novel counter-flow heat and mass exchanger for dew point evaporative cooling. *Applied Thermal Engineering* **28**, 1942-1951, doi:http://dx.doi.org/10.1016/j.applthermaleng.2007.12.006 (2008).
18 Zhao, X., Yang, S., Duan, Z. & Riffat, S. B. Feasibility study of a novel dew point air conditioning system for China building application. *Building and Environment* **44**, 1990-1999, doi:http://dx.doi.org/10.1016/j.buildenv.2009.02.003 (2009).
19 Wu, J. M., Huang, X. & Zhang, H. Numerical investigation on the heat and mass transfer in a direct evaporative cooler. *Applied Thermal Engineering* **29**, 195-201, doi:http://dx.doi.org/10.1016/j.applthermaleng.2008.02.018 (2009).
20 Franco, A., Valera, D. L., Madueño, A. & Peña, A. Influence of water and air flow on the performance of cellulose evaporative cooling pads used in mediterranean greenhouses. *Transactions of the ASABE* **53**, 565-576 (2010).
21 Johnson, D. W., Yavuzturk, C. & Pruis, J. Analysis of heat and mass transfer phenomena in hollow fiber membranes used for evaporative cooling. *Journal of Membrane Science* **227**, 159-171, doi:http://dx.doi.org/10.1016/j.memsci.2003.08.023 (2003).
22 Chen, X., Su, Y., Reay, D. & Riffat, S. Recent research developments in polymer heat exchangers – A review. *Renewable and Sustainable Energy Reviews* **60**, 1367-1386, doi:http://dx.doi.org/10.1016/j.rser.2016.03.024 (2016).

23 Chiari, A. Air humidification with membrane contactors: experimental and theoretical results. *International journal of ambient energy* **21**, 187-195 (2000).
24 Wickramasinghe, S. R., Semmens, M. J. & Cussler, E. L. Hollow fiber modules made with hollow fiber fabric. *Journal of Membrane Science* **84**, 1-14, doi:http://dx.doi.org/10.1016/0376-7388(93)85046-Y (1993).
25 Chen, X. *et al.* Experimental investigations of polymer hollow fibre heat exchangers for building heat recovery application. *Energy and Buildings* **125**, 99-108, doi:http://dx.doi.org/10.1016/j.enbuild.2016.04.083 (2016).
26 Kachhwaha, S. S. & Prabhakar, S. Heat and mass transfer study in a direct evaporative cooler. *Journal of Scientific & Industrial Research* **69**, 705-710 (2010).
27 Zhang, L.-Z. Coupled heat and mass transfer in an application-scale cross-flow hollow fiber membrane module for air humidification. *International Journal of Heat and Mass Transfer* **55**, 5861-5869, doi:http://dx.doi.org/10.1016/j.ijheatmasstransfer.2012.05.083 (2012).
28 Anisimov, S., Pandelidis, D. & Danielewicz, J. Numerical study and optimization of the combined indirect evaporative air cooler for air-conditioning systems. *Energy* **80**, 452-464, doi:https://doi.org/10.1016/j.energy.2014.11.086 (2015).
29 Lin, J. *et al.* Study on dew point evaporative cooling system with counter-flow configuration. *Energy Conversion and Management* **109**, 153-165, doi:https://doi.org/10.1016/j.enconman.2015.11.059 (2016).
30 Jradi, M. & Riffat, S. Experimental and numerical investigation of a dew-point cooling system for thermal comfort in buildings. *Applied Energy* **132**, 524-535, doi:https://doi.org/10.1016/j.apenergy.2014.07.040 (2014).
31 Zhang, L.-Z. Heat and mass transfer in a randomly packed hollow fiber membrane module: A fractal model approach. *International Journal of Heat and Mass Transfer* **54**, 2921-2931, doi:https://doi.org/10.1016/j.ijheatmasstransfer.2011.03.005 (2011).
32 Zhan, C. *et al.* Comparative study of the performance of the M-cycle counter-flow and cross-flow heat exchangers for indirect evaporative cooling – Paving the path toward sustainable cooling of buildings. *Energy* **36**, 6790-6805, doi:https://doi.org/10.1016/j.energy.2011.10.019 (2011).
33 Anisimov, S. & Pandelidis, D. Numerical study of the Maisotsenko cycle heat and mass exchanger. *International Journal of Heat and Mass Transfer* **75**, 75-96, doi:https://doi.org/10.1016/j.ijheatmasstransfer.2014.03.050 (2014).
34 Elmer, T., Worall, M., Wu, S. & Riffat, S. An experimental study of a novel integrated desiccant air conditioning system for building applications. *Energy and Buildings* **111**, 434-445, doi:http://dx.doi.org/10.1016/j.enbuild.2015.11.065 (2016).